

Effect of buffer layer Bi_2Te_3 on anisotropic Gilbert damping of Fe/α-GeTe on Al_2O_3 substrate

Qing-Lin Yang(杨庆林), Xu Yang(杨旭), Xiang-Qun Zhang(张向群), Wei He(何为), and Zhao-Hua Cheng(成昭华)
Citation: Chin. Phys. B, 2026, 35 (**6**): 067601. DOI: 10.1088/1674-1056/ae15f6
http://cpb.iphy.ac.cn; http://iopscience.iop.org/cpb

What follows is a list of articles you may be interested in

Spin wave resonance frequency in bilayer ferromagnetic films with the biquadratic exchange interaction

Xiaojie Zhang(张晓洁), Yuting Wang(王雨汀), Yanqiu Chang(常艳秋), Huan Wang(王焕), Jianhong Rong(荣建红), and Guohong Yun(云国宏)
Chin. Phys. B, 2024, 33 (**9**): 097601. DOI: 10.1088/1674-1056/ad50bc

Eigenstates and temporal dynamics in cavity optomagnonics

Yun-Jing Ding(丁云静) and Yang Xiao(肖杨)
Chin. Phys. B, 2023, 32 (**10**): 107601. DOI: 10.1088/1674-1056/acf039

Spin pumping by higher-order dipole-exchange spin-wave modes

Peng Wang(王鹏)
Chin. Phys. B, 2023, 32 (**3**): 037601. DOI: 10.1088/1674-1056/ac8922

Theoretical investigation of ferromagnetic resonance in a ferromagnetic thin film with external stress anisotropy

Jieyu Zhou(周婕妤), Jianhong Rong(荣建红), Huan Wang(王焕), Guohong Yun(云国宏), Yanan Wang(王娅男), and Shufei Zhang(张舒飞)
Chin. Phys. B, 2022, 31 (**1**): 017601. DOI: 10.1088/1674-1056/ac1b86

Controlled vapor growth of 2D magnetic Cr_2Se_3 and its magnetic proximity effect in heterostructures

Danliang Zhang(张丹亮), Chen Yi(易琛), Cuihuan Ge(葛翠环), Weining Shu(舒维宁), Bo Li(黎博), Xidong Duan(段曦东), Anlian Pan(潘安练), and Xiao Wang(王笑)
Chin. Phys. B, 2021, 30 (**9**): 097601. DOI: 10.1088/1674-1056/ac0cd9

Effect of buffer layer Bi_2Te_3 on anisotropic Gilbert damping of Fe/α-GeTe on Al_2O_3 substrate

Qing-Lin Yang(杨庆林)[1,2], Xu Yang(杨旭)[1,3], Xiang-Qun Zhang(张向群)[1], Wei He(何为)[1], and Zhao-Hua Cheng(成昭华)[1,2,3,†]

[1] *Beijing National Laboratory for Condensed Matter Physics, Institute of Physics, Chinese Academy of Sciences, Beijing* 100190, *China*
[2] *School of Physical Sciences, University of Chinese Academy of Sciences, Beijing* 100049, *China*
[3] *Songshan Lake Materials Laboratory, Dongguan* 523808, *China*

(Received 27 August 2025; revised manuscript received 26 September 2025; accepted manuscript online 22 October 2025)

The α-GeTe is a typical ferroelectric Rashba semiconductor (FERSC) that has attracted a lot of attention in spintronics. The Fe/α-GeTe grown on Si substrates has anisotropic Gilbert damping. However, the effect of Al_2O_3, as another common substrate, remains unknown when α-GeTe is grown on it. Here, we fabricated α-GeTe thin films using Al_2O_3 substrates. The α-GeTe directly grown on Al_2O_3 exhibits an in-plane polycrystalline structure. A Bi_2Te_3 buffer layer can make the α-GeTe exhibit a single-crystal feature. The anisotropic Gilbert damping of FM layers is present in Fe/α-GeTe/Bi_2Te_3/Al_2O_3 and vanished in Fe/α-GeTe/Al_2O_3. Our finding illustrates that α-GeTe growth on Al_2O_3 with a Bi_2Te_3 buffer layer can serve as a suitable platform for anisotropic research. Our work paves the way for the application of the Al_2O_3-based α-GeTe thin films in anisotropic electronics.

Keywords: ferroelectric Rashba semiconductor, anisotropic Gilbert damping, buffer layer

PACS: 76.50.+g, 73.20.At, 75.76.+j, 75.40.Gb

DOI: 10.1088/1674-1056/ae15f6 **CSTR:** 32038.14.CPB.ae15f6

1. Introduction

Germanium telluride (GeTe) is a typical ferroelectric Rashba semiconductor (FERSC). Below the Curie temperature of 700 K, α-GeTe exhibits the bulk Rashba effect arising from the ferroelectric polarization caused by inversion symmetry breaking within the bulk of the material.[1–3] Recent studies found that GeTe has the largest Rashba parameter α_R.[2,4–6] Thus, α-GeTe has attracted a lot of attention in spintronics for potential applications.[7–13] Besides the Rashba effect, the cubic Dresselhaus effect plays an important role in α-GeTe, which produces a three-fold symmetry out-of-plane spin component and a six-fold symmetry warping of the Fermi surface in the band structure.[8,14,15] The anisotropic band structure means that α-GeTe is an alternative material for anisotropic research. One of the crucial issues is anisotropic Gilbert damping in spintronics, which has been observed in several systems.[16–25] In Fe/α-GeTe heterostructures, anisotropic Gilbert damping can be induced by the spin pumping effect. The spin current can transfer angular momentum from the Fe layer to the α-GeTe layer, further enhancing the Gilbert damping of the Fe.[12,26–30] The spin current will suffer anisotropic scattering intensity at the interface between Fe and α-GeTe, which is related to the anisotropic band structure of the α-GeTe layer.[8,31]

The growth of heterostructures on Si substrates is a very common choice.[32] However, the Si substrate has some disadvantages. For example, its high electrical conductivity limits its application in electrical transport measurements. Compared to Si, Al_2O_3 substrates have benefits such as low dielectric loss, high thermal conductivity, high electrical resistance, etc.[33,34] Al_2O_3 substrates have also been used to grow GeTe thin films in different works.[7,35] Among them, the topological insulator Bi_2Te_3 acted as a buffer layer to reduce the mismatch between α-GeTe and Al_2O_3, which can optimize the thermoelectric performance.[35] However, whether the anisotropic feature still exists in α-GeTe when grown on Al_2O_3 remains unknown.

Here, we fabricated α-GeTe thin films on Al_2O_3 substrates and compared the growth conditions with and without a Bi_2Te_3 buffer layer. Reflection high-energy electron diffraction (RHEED) and x-ray diffraction (XRD) measurements were performed to confirm the crystal orientation of the thin films. The results reveal that the 30-nm α-GeTe thin films grown directly on Al_2O_3 have a random in-plane orientation. However, with a 2 quintuple layers (QLs) Bi_2Te_3 buffer layer, the α-GeTe thin films exhibit a single-crystal feature. In addition, the electronic structure was measured via angle-resolved photoemission spectroscopy (ARPES), and the temperature dependence of the resistivity ρ_{xx} was measured. Both GeTe thin films with and without a buffer layer show Rashba-split bands and have similar transport characteristics. Furthermore, an FM Fe layer was grown on the two types of GeTe thin films, and the Gilbert damping was measured via ferromagnetic resonance (FMR) measurements. The Gilbert

†Corresponding author. E-mail: zhcheng@iphy.ac.cn

© 2026 Chinese Physical Society and IOP Publishing Ltd. All rights, including for text and data mining, AI training, and similar technologies, are reserved.

damping in the heterostructure without Bi_2Te_3 is isotropic, but anisotropic in the case with Bi_2Te_3. Our findings illustrate that α-GeTe growth on Al_2O_3 with a Bi_2Te_3 buffer layer can act as a platform for performing anisotropic research. Our work paves the way for the application of Al_2O_3-based α-GeTe thin films in anisotropic electronics.

2. Methods

The α-GeTe thin films were grown by molecular beam epitaxy (MBE) on Al_2O_3 (0001) substrates. The base pressure of the growth chamber is about 1.0×10^{-10} mbar (1 bar = 10^5 Pa). The substrates were wet-chemically cleaned and annealed at 1150 °C in O_2 for 3 hours to produce a terrace-step-like surface structure. The prepared substrates were transferred to the MBE chamber and heated at 800 °C to degas. Thin Bi_2Te_3 films were grown by evaporation of high-purity Bi (99.999%) and Te (99.999%) from Knudsen cells onto Al_2O_3 (0001). The temperatures of Bi, Te, and the substrate were 420 °C, 300 °C, and 250 °C. The thickness of Bi_2Te_3 is determined via x-ray reflectivity (XRR). A Bi_2Te_3 layer was grown for 30 minutes, and the thickness was measured via XRR, as shown in Fig. S3 in supporting information. The thickness of the thin film is related to the period of oscillations in XRR measurements, and the period of oscillations of the fitting line is consistent with the experimental data in Fig. S3. The fitted thickness is 14.3 nm; thus, the growth rate is 0.48 nm/min. The thickness of a 2 QL Bi_2Te_3 is about 2.1 nm. Therefore, by controlling the growth time of Bi_2Te_3 to 4.4 min, a 2 QL Bi_2Te_3 can be fabricated. Then, the GeTe was deposited on top of the Bi_2Te_3 and Al_2O_3 (0001) directly. α-GeTe films were also grown by coevaporating Ge (99.99%) and Te. The temperatures of Ge, Te, and the substrate were 1150 °C, 300 °C, and 100 °C. The 10-nm Fe layers were grown onto the α-GeTe, and a 2-nm Cu capping layer was deposited on top to protect the Fe layers.

The electronic structures of the thin films were collected by ARPES with a photon energy of 21.2 eV at room temperature. The base pressure of the ARPES chamber was about 3.0×10^{-11} mbar. The energy and angle resolution of the Scienta DA30L electron energy analyzer were better than 20 meV and 0.01 $Å^{-1}$, respectively.

FMR measurements were performed using a vector network analyzer (VNA, model Agilent N5224A) to measure the microwave transmission parameter S_{21}. The samples were placed face down onto a homemade coplanar waveguide (CPW). For the angular-dependent FMR measurements, the in-plane magnetization direction was changed with an azimuthal angle ϕ_H. The measurement was conducted at room temperature. The probing RF power was set at -10 dBm.

3. Results and discussion

The samples α-GeTe (30 nm) with and without a Bi_2Te_3 buffer layer were fabricated; the thickness of the Bi_2Te_3 buffer layer is 2 QLs. More details are shown in Section 2. As shown in Fig. 1(a), the $\omega/2\theta$ mode was adopted in XRD measurements to detect the crystal orientation along the z axis, and the RHEED measurements were conducted with the electron beam incident along different directions, which can distinguish the in-plane (xy plane) crystal orientation. The results of the sample α-GeTe (30 nm) without Bi_2Te_3 are shown in Fig. 1(b); the XRD pattern shows the peak coming from the Al_2O_3 substrate corresponding to (0001). In addition, the peaks of α-GeTe (0003) and (0006) are observed, which means the crystal orientation along the z axis is well aligned. However, in Fig. 1(c), the RHEED patterns show that the electron beam was incident along different directions, but the patterns include identical streaks, even when the incident direction is not a high-symmetry direction. The isotropic RHEED patterns indicate the crystal orientation in the xy plane of α-GeTe directly grown on Al_2O_3 substrate is random in different crystalline grains. To further confirm the orientation of GeTe, the intensity of the RHEED patterns in Figs. 1(f)–1(g) was extracted, as shown in Fig. S1 in supporting information. The peak positions were labeled with the red lines. When the incident direction was changed in RHEED measurements, the peak positions were identical and totally isotropic, even when the incident direction is the non-high-symmetry direction, which illustrates the random orientation of GeTe directly grown on Al_2O_3. For comparison, XRD and RHEED measurements of α-GeTe (30 nm) with a Bi_2Te_3 buffer layer were carried out, as shown in Fig. 1(d). In Fig. 2(e), the XRD pattern shows the same peaks, including α-GeTe (0003), (0006), Al_2O_3 (0001), and the peak (00015) of the Bi_2Te_3 buffer layer, indicating the crystal orientation along the z axis of the sample is still well aligned. The RHEED patterns show many different features in Fig. 1(f). When the electron beam is incident along the $[11\bar{2}0]$ and $[10\bar{1}0]$ directions of α-GeTe, the patterns show different features. The upper pattern shows five streaks and the lower shows three, and the distance between the streaks is different, due to the different lattice parameters. This feature means the α-GeTe with a Bi_2Te_3 buffer layer has a single crystal feature.[36] The RHEED pattern of the Bi_2Te_3 buffer layer is displayed in Fig. 1(g) to illustrate the epitaxial growth of α-GeTe on Bi_2Te_3. Fig. S2 in supporting information shows the crystal structure of GeTe/Bi_2Te_3/Al_2O_3, and the in-plane orientation $[10\bar{1}]$ of the three layers is parallel to each other in epitaxial growth. The difference in the in-plane crystal orientation of these two samples is caused by lattice mismatch. The in-plane lattice parameters of GeTe, Bi_2Te_3, and Al_2O_3 are 4.1546 Å, 4.38 Å, and 4.758 Å, respectively.

Thus, the mismatch between GeTe and Al_2O_3 is about 12% and the mismatch between GeTe and Bi_2Te_3 is 5%. Therefore, the Bi_2Te_3 buffer layer can effectively decrease the mismatch to 5% and eliminate the formation of twin structures, as the previous work reported.[35]

The band structure of α-GeTe grown on Al_2O_3 substrates was measured via ARPES. The ARPES spectra of α-GeTe grown on Al_2O_3 substrates without and with the buffer layer are given in Figs. 2(c) and 2(b). The ARPES spectrum of α-GeTe grown on an Si substrate is also given in Fig. 2(a) for comparison. In Fig. 2(c), the ARPES spectrum exhibits a bulk Rashba band. As discussed above, the crystal orientation along the z axis of α-GeTe grown on an Al_2O_3 substrate is well aligned, which corresponds to the ferroelectric polarization direction and ensures the Rashba splitting band exists in the ARPES measurements. However, due to the in-plane crystal orientation being random in different crystalline grains, the spectrum in Fig. 2(c) is the sum of the spectra in different cross directions, which results in the broadening of the spectra. In Figs. 2(a) and 2(b), the spectra have the same characteristics. Both ARPES spectra show distinguishable surface states (SS) and bulk states (BS) in the cross direction *A*–*Z*–*A*, as in previous works,[2,4] which means the GeTe grown on Al_2O_3 substrates with the buffer layer still has the Rashba splitting band. Meanwhile, the spectrum in Fig. 2(b) is clearer than that in Fig. 2(c), led by the improvement of crystalline quality. To further explore the effect of the buffer layer on the transport properties, the temperature-dependent longitudinal resistivity of the sample with and without Bi_2Te_3 was measured. The result is displayed as the black and blue lines in Fig. 2(d). Both longitudinal resistivities increase with temperature, suggesting metallic behavior. For comparison, the temperature-dependent longitudinal resistivity of GeTe/Al_2O_3 reported in Ref. [7] is displayed in Fig. 2(d) as the red line. The same behavior illustrates that the 2 QLs Bi_2Te_3 buffer layer does not affect the transport feature of 30-nm α-GeTe.

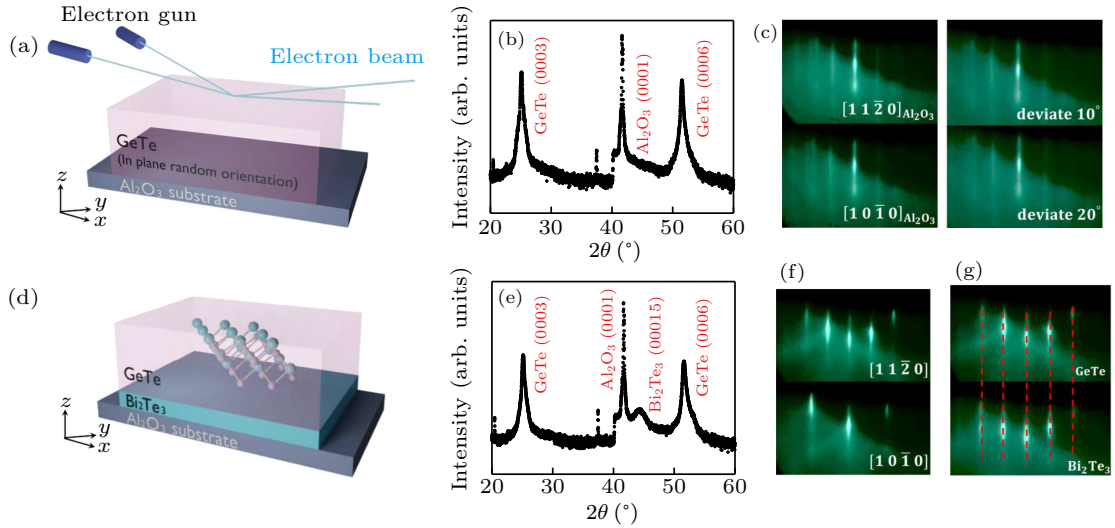


Fig. 1. (a) The schematic diagram of the sample α-GeTe grown on Al_2O_3. The GeTe is randomly oriented in the *xy* plane, and the orientation is well aligned along the z axis. (b) The XRD pattern of α-GeTe/Al_2O_3. (c) The left two panels are the RHEED patterns of α-GeTe incident along the high-symmetry directions, the upper panel is incident along $[11\bar{2}0]$ of Al_2O_3, and the lower panel is along $[10\bar{1}0]$ of Al_2O_3. The right two panels are the RHEED patterns of α-GeTe incident along the non-high-symmetry directions. The direction of the upper one is deviated 10° from $[10\bar{1}0]$, and deviated 20° from $[10\bar{1}0]$ in the lower one. (d) The schematic diagram of the RHEED and XRD measurements for sample α-GeTe grown on Al_2O_3 with a Bi_2Te_3 buffer layer. The GeTe has a single crystal feature. (e) The XRD pattern of α-GeTe/Bi_2Te_3/Al_2O_3. (f) The RHEED patterns of α-GeTe, the upper panel is incident along $[11\bar{2}0]$, and the lower panel is along $[10\bar{1}0]$. (g) The RHEED patterns of α-GeTe (upper panel) and Bi_2Te_3 (lower panel) along $[11\bar{2}0]$, the red dash lines mean the epitaxy growth between α-GeTe and Bi_2Te_3.

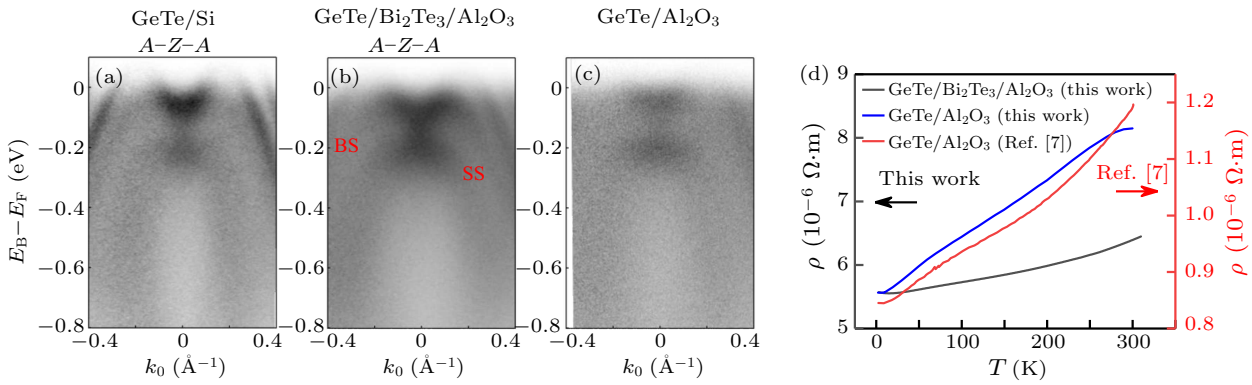


Fig. 2. (a)–(c) The ARPES spectra of GeTe/Si, GeTe/Bi_2Te_3/Al_2O_3, and GeTe/Al_2O_3, respectively. (d) The temperature-dependent longitudinal resistivity of GeTe/Bi_2Te_3/Al_2O_3 and GeTe/Al_2O_3.

The Fe/α-GeTe grown on Si substrates exhibits anisotropic Gilbert damping, which is related to the anisotropic band structure. However, the α-GeTe grown on the Al_2O_3 has a random in-plane crystal orientation, which might affect the anisotropic research. Therefore, a ferromagnetic Fe layer was grown, and the angle-dependent Gilbert damping was measured via the vector-network-analyzer ferromagnetic resonance (VNA-FMR) technique. Figure 3(a) shows the schematic diagram of the angle-dependent magnetization dynamics measurement. The samples were placed face-down on the coplanar waveguide; the applied magnetic field $\boldsymbol{H}$, which determines the magnetic direction of the Fe film, was aligned along the azimuthal angle ϕ_H with respect to the *Z*–*A* direction. The magnetic resonance is detected in the microwave frequency range from 5 GHz to 18 GHz. One of the *S* parameters of the VNA, S_{21}, was measured and the real part $\mathrm{Re}\,|S_{21}|$ was extracted, as shown in Fig. 3(b). Figure 3(c) shows the $\mathrm{Re}\,|S_{21}|$ versus $\boldsymbol{H}$ spectrum at different frequencies f. The $\boldsymbol{H}$-dependent resonance spectra $\mathrm{Re}\,|S_{21}|$ at a fixed frequency f can be described using[8]

$$\mathrm{Re}\,|S_{21}|(H) = a_1 + b_1 \times \frac{\Delta H^2}{(H-H_{\mathrm{res}})^2+\Delta H^2} + b_2 \times \frac{\Delta H\,(H-H_{\mathrm{res}})}{(H-H_{\mathrm{res}})^2+\Delta H^2}, \tag{1}$$

where H_{res} is the resonance field and ΔH is the full width at half maximum linewidth at resonance frequency f; b_1 and b_2 are the symmetric and antisymmetric magnitudes, respectively. By fitting $\mathrm{Re}\,|S_{21}|$ using Eq. (1), the ΔH at different frequencies f can be extracted. Figure 3(d) shows the FMR linewidth ΔH versus resonance frequency f for the Fe/α-GeTe/Bi_2Te_3/Al_2O_3 sample at different angular ϕ_H. The Gilbert damping can be fitted using[8,37]

$$\mu_0\Delta H = \mu_0\Delta H_0 + \frac{2\pi\alpha}{\gamma} f, \tag{2}$$

where γ is the gyromagnetic ratio, $\mu_0\Delta H_0$ is the inhomogeneous broadening due to disorder, and α is the Gilbert damping. The red lines in Fig. 3(d) are the best-fitting lines. The angle-dependent α of the Fe/α-GeTe/Al_2O_3 sample was extracted and is displayed in Fig. 4(a). It shows only a uniaxial anisotropy, which is caused by the oblique incidence when the ferromagnetic layers were deposited on the GeTe.[38,39] The Gilbert damping does not have six-fold symmetry.

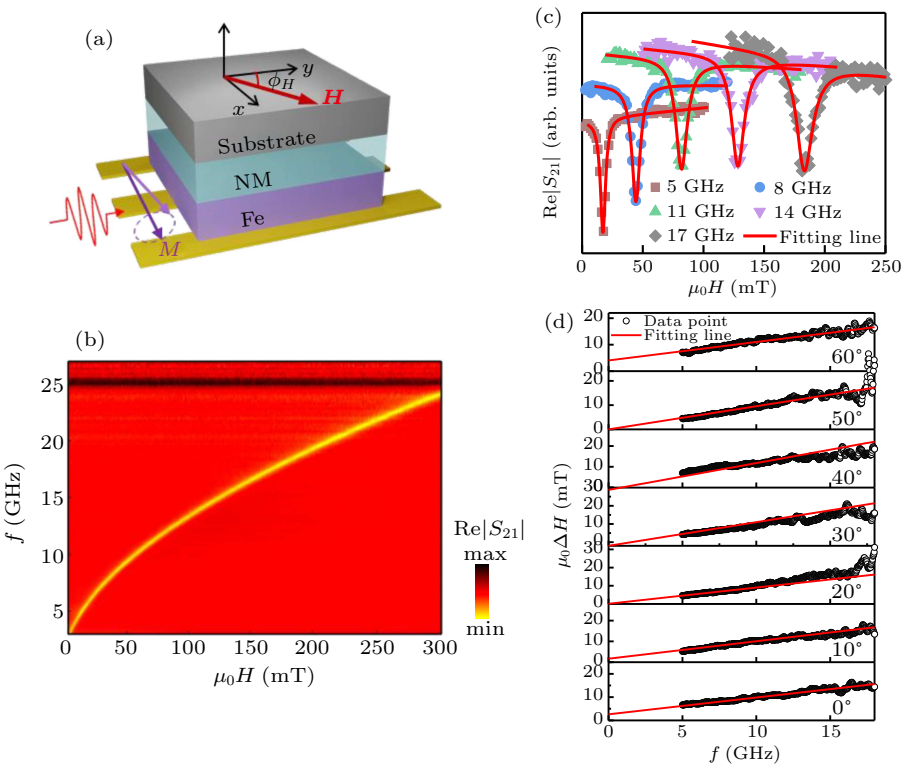


Fig. 3. (a) The schematic diagram of VNA-FMR measurement configuration. The *y* corresponding to the *Z*–*A* direction of GeTe. (b) The $\mathrm{Re}\,|S_{21}|$ signal of VNA. (c) $\mathrm{Re}\,|S_{21}|$ versus magnetic field *H* at different frequencies. (c) Resonance linewidth $\mu_0\Delta H$ versus frequency *f* along the separate azimuthal direction with $\phi_H = 0°, 10°, 20°, 30°, 40°, 50°, 60°$. The red lines are the linear fitting lines.

By contrast, the angle-dependent α of the sample Fe/α-GeTe/Bi_2Te_3/Al_2O_3 is shown in Fig. 4(b). As a result, the Gilbert damping α exhibits a sixfold symmetry. This result is consistent with the previous report and illustrates that the anisotropic Gilbert damping in Fe/α-GeTe is not affected by the substrate.[8] In addition, the α in both samples is about 0.015, much larger than that in a pure Fe thin film, which is about 0.006. The enhancement means the existence of a spin pumping effect.[8] The anisotropic Gilbert damping originates from the anisotropic spin current injection at the interface between Fe and α-GeTe. When the injecting polarization direction of spin current is along the *Z*–*A* direction, the possibil-

ity of scattering is stronger than that along the *Z*–*U*; thus, the Gilbert damping along the *Z*–*A* direction is smaller.[8] When the α-GeTe is grown on Al_2O_3, the crystal orientation in different crystalline grains is random. Thus, when the spin current is injected into the α-GeTe from Fe, the scattering intensity suffered is the average of all directions, which is isotropic. Therefore, the Gilbert damping is isotropic.

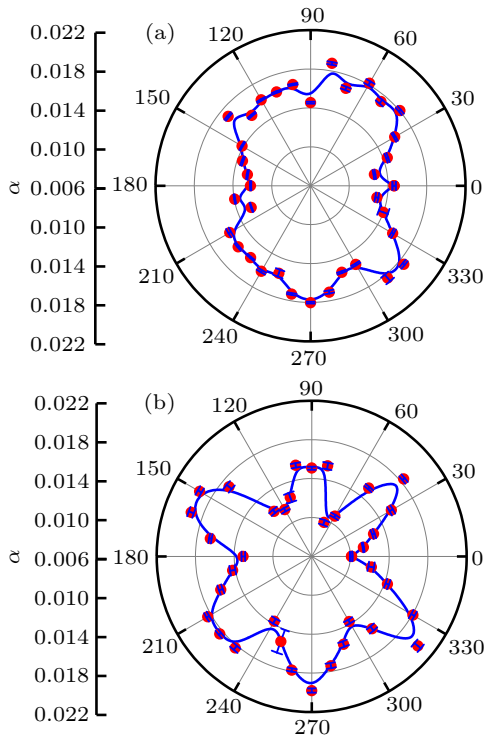


Fig. 4. (a) The Gilbert damping factor α versus azimuthal ϕ_H in Fe/GeTe/Al_2O_3. (b) The Gilbert damping α versus azimuthal ϕ_H in Fe/GeTe/Bi_2Te_3/Al_2O_3.

4. Conclusion

In conclusion, we fabricated the α-GeTe grown on Al_2O_3 substrates with and without a Bi_2Te_3 buffer layer and investigated the crystal orientation of the samples. The α-GeTe grown on Al_2O_3 substrates directly has a well-aligned crystal orientation along the z axis, but the in-plane orientation is random in different crystalline grains. The Bi_2Te_3 buffer layer can significantly improve this by decreasing the mismatch between α-GeTe and Al_2O_3. The buffer layer makes α-GeTe become a single crystal. Furthermore, both of these show a Rashba splitting band and metallic behaviors, illustrating that the Bi_2Te_3 buffer layer does not affect the transport feature. In addition, the anisotropic Gilbert damping was present in Fe/α-GeTe/Bi_2Te_3/Al_2O_3 and disappeared in Fe/α-GeTe/Al_2O_3, indicating the random orientation in α-GeTe is a disadvantage for anisotropic research. Our method provides a method to conduct anisotropic electrical transport based on GeTe, which paves the way for the application of GeTe in anisotropic electronics.

Acknowledgements

Project supported by the National Key Research Program and Development of China (Grant Nos. 2022YFA1403302 and 2024YFA1408702), the National Natural Sciences Foundation of China (Grant Nos. U22A20115 and 52031015), the Young Scientists Fund of the National Natural Science Foundation of China (Grant No. 12404140), and the China Postdoctoral Science Foundation (Grant No. 2023M732518).

References

[1] Ishizaka K, Bahramy M S, Murakawa H, *et al.* 2011 *Nat. Mater.* **10** 521
[2] Liebmann M, Rinaldi C, Di Sante D, *et al.* 2016 *Adv. Mater.* **28** 560
[3] Wang Y, Lei Z, Zhang J, Tao X, Hua C and Lu Y 2023 *Chin. Phys. Lett.* **40** 117102
[4] Krempaský J, Volfová H, Muff S, Pilet N, Landolt G, Radović M, Shi M, Kriegner D, Holý V, Braun J, Ebert H, Bisti F, Rogalev V A, Strocov V N, Springholz G, Minár J and Dil J H 2016 *Phys. Rev. B* **94** 205111
[5] Rinaldi C, Varotto S, Asa M, Slawinska J, Fujii J, Vinai G, Cecchi S, Di Sante D, Calarco R, Vobornik I, Panaccione G, Picozzi S and Bertacco R 2018 *Nano Lett.* **18** 2751
[6] Yang X, Li X M, Li Y, Li Y, Sun R, Liu J N, Bai X, Li N, Xie Z K, Su L, Gong Z Z, Zhang X Q, He W and Cheng Z 2021 *Nano Lett.* **21** 77
[7] Li Y, Li Y, Li P, Fang B, Yang X, Wen Y, Zheng D X, Zhang C H, He X, Manchon A, Cheng Z H and Zhang X X 2021 *Nat. Commun.* **12** 540
[8] Yang X, Qiu L, Li Y, Xue H P, Liu J N, Sun R, Yang Q L, Gai X S, Wei Y S, Comstock A H, Sun D, Zhang X Q, He W, Hou Y and Cheng Z H 2023 *Phys. Rev. Lett.* **131** 186703
[9] Rojas Sanchez J C, Vila L, Desfonds G, Gambarelli S, Attane J P, De Teresa J M, Magen C and Fert A 2013 *Nat. Commun.* **4** 2944
[10] Bihlmayer G, Noël P, Vyalikh D V, Chulkov E V and Manchon A 2022 *Nat. Rev. Phys.* **4** 642
[11] Noël P, Trier F, Arche L V M, Bréhin J, Vaz D C, Garcia V, Fusil S, Barthélémy A, Vila L, Bibes M and Attané J P 2020 *Nature* **580** 483
[12] Rinaldi C, Rojas-Sánchez J C, Wang R N, Fu Y, Oyarzun S, Vila L, Bertoli S, Asa M, Baldrati L, Cantoni M, George J M, Calarco R, Fert A and Bertacco R 2016 *APL Mater.* **4** 032501
[13] Varotto S, Nessi L, Cecchi S, *et al.* 2021 *Nat. Electron.* **4** 740
[14] Di Sante D, Barone P, Bertacco R and Picozzi S 2013 *Adv. Mater.* **25** 509
[15] Sánchez-Barriga J, Scholz M R, Golias E, Rienks E, Marchenko D, Varykhalov A, Yashina L V and Rader O 2014 *Phys. Rev. B* **90** 195413
[16] Chen L, Mankovsky S, Wimmer S, Schoen M A W, Körner H S, Kronseder M, Schuh D, Bougeard D, Ebert H, Weiss D and Back C H 2018 *Nat. Phys.* **14** 490
[17] Li Y, Zeng F, Zhang S S L, Shin H, Saglam H, Karakas V, Ozatay O, Pearson J E, Heinonen O G, Wu Y, Hoffmann A and Zhang W 2019 *Phys. Rev. Lett.* **122** 117203
[18] Chen L, Mankovsky S, Kronseder M, Schuh D, Prager M, Bougeard D, Ebert H, Weiss D and Back C H 2023 *Phys. Rev. Lett.* **130** 046704
[19] Xu H, Chen H, Zeng F, Xu J, Shen X and Wu Y 2023 *Phys. Rev. Appl.* **19** 024030
[20] Chen K and Zhang S 2015 *Phys. Rev. Lett.* **114** 126602
[21] Sun R, Sun Y B, Li N, Xue H P, Li Y, Yang X, Li Y, Comstock A H, Sun D, He W, Zhang X Q and Cheng Z H 2024 *Phys. Rev. B* **110** 024408
[22] Yang P T, Liu R X, Yuan Z and Liu Y 2022 *Phys. Rev. B* **106** 134409
[23] Gilmore K, Stiles M D, Seib J, Steiauf D and Fähnle M 2010 *Phys. Rev. B* **81** 174414
[24] Fähnle M, Steiauf D and Seib J 2008 *J. Phys. D: Appl. Phys.* **41** 164014
[25] Safonov V L 2002 *J. Appl. Phys.* **91** 8653
[26] Tserkovnyak Y, Brataas A and Bauer G E W 2002 *Phys. Rev. Lett.* **88** 117601
[27] Tserkovnyak Y, Brataas A, Bauer G E W and Halperin B I 2005 *Rev. Mod. Phys.* **77** 1375
[28] Tserkovnyak Y, Brataas A and Bauer G E W 2002 *Phys. Rev. B* **66** 224403
[29] Rojas-Sánchez J C, Oyarzún S, Fu Y, Marty A, Vergnaud C, Gambarelli S, Vila L, Jamet M, Ohtsubo Y, Taleb-Ibrahimi A, Le Fèvre P, Bertran F, Reyren N, George J M and Fert A 2016 *Phys. Rev. Lett.* **116** 096602
[30] Fanchiang Y T, Chen K H M, Tseng C C, Chen C C, Cheng C K, Yang S R, Wu C N, Lee S F, Hong M and Kwo J 2018 *Nat. Commun.* **9** 223

[31] Liu J N, Xue H P, Deng Z, Yang Q L, Li X M, Bai X D, Yang X, Yang P T, Gao Y H, He W, Zhang X Q and Cheng Z H 2025 *Phys. Rev. Lett.* **134** 236204
[32] Ding X, Li Y, Kang C, Song Y H and Zhang W 2024 *Chin. Phys. B* **33** 117301
[33] Liu W, Shen Y, Li D, Ouyang X, Liu Q and Wang S 2025 *Ceram. Int.* **51** 5000
[34] Bansal and Narottam P 2005 *Handbook of Ceramic Composites* (New York: Springer) p. 1
[35] Chen T, Xiang Q, Ge H, Li Z, Yan F, Cheng J, Hong M, Luo Y, Yang J, Liu Y, Liu W and Tang X 2024 *Mater. Today Energy* **42** 101550
[36] Wang R, Boschker J E, Bruyer E, Sante D D, Picozzi S, Perumal K, Giussani A, Riechert H and Calarco R 2014 *J. Phys. Chem. C* **118** 29724
[37] Zhan J, Wang Y, Wang X, Zhang H, Zhu S, Zhang L, Tao L, Sui Y, He W, Wan C, Han X, Belotelov V I and Song B 2024 *Chin. Phys. B* **33** 107505
[38] Bubendorff J L, Zabrocki S, Garreau G, Hajjar S, Jaafar R, Berling D, Mehdaoui A, Pirri C and Gewinner G 2006 *Europhys. Lett.* **75** 119
[39] Li Y, Li Y, Liu Q, Yuan Z, Zhan Q F, He W, Liu H L, Xia K, Yu W, Zhang X Q and Cheng Z H 2019 *New J. Phys.* **21** 123001